Supplementary Materials for

Ribosome stalling induced by mutation of a CNS-specific tRNA causes neurodegeneration

Ryuta Ishimura, Gabor Nagy, Ivan Dotu, Huihao Zhou, Xiang-Lei Yang,

Paul Schimmel, Satoru Senju, Yasuharu Nishimura, Jeffrey H. Chuang,

Susan L. Ackerman*

*Corresponding author. E-mail: susan.ackerman@jax.org

This PDF file includes:

Materials and Methods
Figs. S1 to S17
Tables S1, S3, and S4
Full Reference List

Other Supplementary Materials for this manuscript include the following:

Table S2
Movie S1

Materials and Methods

Mice

Genetic mapping of the *nmf205* mutation was performed in an intercross with BALB/cByJ mice using polymorphic microsatellite and SNP markers. The phenotype of F2 mice was assessed at 6-8 weeks of age. Initial mapping of *Mod205* was also performed in an intercross of C57BL/6J (B6J)-*nmf205*$^{+/-}$ and BALB/cBy mice. *Mod205* fine mapping was performed by intercrossing B6J.BALB$^{D1Mit399\text{-}D1Mit291}$ or BALB.B6J$^{D1Mit399\text{-}D1Mit291}$ mice that were heterozygous for B6J and BALB alleles in the congenic region. Mice with recombination events in this region of Chromosome 1 were crossed to B6J-*nmf205*$^{+/-}$ mice and F1 mice were backcrossed to B6J-*nmf205*$^{+/-}$ mice to generate *nmf205*$^{-/-}$ carrying the recombinant chromosome. Ataxia and cerebellar degeneration were assessed in these mice at 6-8 weeks of age. The *Gtpbp2* targeted allele was generated by replacing a 1.6 kb genomic region containing exons 4, 5, and part of exon 6, with a neo resistance cassette in TT2 ES cells (*20*). Heterozygous mice were bred to B6J mice for 10 generations to generate the B6J.Cg-*Gtpbp2* line used in this study. To generate B6J.B6N-*n-Tr20* mice, B6J and C57BL/6NJ (B6N) mice were intercrossed and mice carrying the B6N allele of *n-Tr20* were backcrossed to B6J mice for 5 generations prior to intercrossing. To generate Tg(n-Tr20^{B6N}) transgenic mice a 1.2 kb PCR fragment containing the *n-Tr20* gene was amplified from B6N genomic DNA and injected into the pronuclei of B6J zygotes. To assess expression of the transgene, northern blots were performed using tissues collected from 1-month-old transgenic mice. Mice carrying the transgene were test mated to B6J-*nmf205*$^{+/-}$ mice to generate *nmf205*$^{-/-}$ mice carrying the transgene. Primer sequences for genotyping are indicated in table S2R. The Jackson Laboratory Animal Care and Use Committee approved all animal protocols.

Histology and immunohistochemistry

Mice were intracardically perfused with Bouin's fixative for hematoxylin and eosin staining or 4% paraformaldehyde (PFA), for immunohistochemistry. Cleaved caspase-3 immunostaining and TUNEL assays were performed as previously described (*21*). Eyes and optic nerves were fixed overnight in 1.2% PFA and 0.8% glutaraldehyde in 0.1M phosphate buffer and embedded in resin. Sections were stained with hematoxylin and eosin or *p*-phenylenediamine staining. For immunofluorescence, eyes were fixed in 4% PFA. Cryosections were incubated with mouse monoclonal antibodies to calretinin (Millipore) or calbindin (Sigma Aldrich), or with rabbit or goat polyclonal antibodies to PKCα (Sigma Aldrich), or Chx10 (Santa Cruz Biotechnology) at 1:200 dilutions. Expression was visualized with Alexa Fluor 488- or 555-labeled donkey secondary antibodies against rabbit and goat or mouse antibodies, respectively. At least 3 mice for each time point and genotype were analyzed.

Northern blot and tRNA aminoacylation analysis

Total RNA was extracted using Trizol reagent (Life Technologies). For tRNA Northern analysis, total RNA was loaded on denaturing 15% polyacrylamide gels and blotted onto Hybond-N+ membranes (GE Healthcare Life Sciences). The membrane was hybridized with 5' end-labeled DNA oligo probes (table S2R) at 55 ºC in a hybridization buffer containing 6x SSC, 0.01M sodium phosphate, 1mM EDTA, 0.25% SDS and 100 μg/ml

salmon sperm DNA. Blots were washed with increasing stringency beginning with 6x SSC, 0.2% SDS at 55 ºC and ending with washes in 2x SSC, 0.1% SDS at 65 ºC. Density of bands on scanned X-ray films was determined by ImageJ (NIH) software. When using pooled DNA oligo probes (table S2R), membranes were hybridized at 60°C in a buffer containing 3M tetramethylammonium chloride (TMACl) instead of SSC.

For mRNA Northern analysis, total RNA was enriched for poly(A)+ RNA using the Oligotex kit (Qiagen). Enriched RNA was then loaded on denaturing 1% agarose gels and capillary blotted onto Hybond-N+ membranes. The membrane was hybridized with probes generated with Prime-It II Random Primer Labeling Kit (Stratagene) at 42 ºC in a buffer containing 5x SSC, 5x Denhardt's reagent, 50% formamide, 0.5% SDS, 10% dextran sulfate, and 100 μg/ml salmon sperm DNA. Blots were washed with increasing stringency beginning with 2x SSC, 0.1% SDS at room temperature and ending with washes in 0.5x SSC, 0.5% SDS at 65 ºC.

Acylated tRNA was extracted using Trizol and the RNA pellet was dissolved in 10 mM NaOAc pH 5. To deacylate tRNA, the pellet was dissolved in 0.2 M Tris-HCl, pH 9.5 and incubated at 37°C for 2 hours, then precipitated and re-dissolved in 10 mM NaOAc, pH 5. RNA was separated on a 6.5% non-denaturing polyacrylamide gel made with 0.1 M NaOAc pH 5 and blotted. Northern hybridization was performed as described above.

Western blotting

Proteins were extracted in 20 mM Tris-HCl pH7.4 containing 140 mM NaCl, 1% Triton, and proteinase inhibitor (complete cocktail, Roche) and proteins were resolved on SDS-PAGE gels prior to transfer to PVDF membranes. After blocking in 5% skim milk, the blot was probed with rabbit anti-human GTPBP2 raised to the N-terminal peptide (65-165 of 602 amino acid GTPBP2 protein, Sigma-Aldrich) followed by incubation with HRP-conjugated anti-rabbit IgG (1:5,000; Bio-Rad Life Science). Signals were detected with ECL Plus (GE Healthcare Life Sciences).

Co-immunoprecipitation and GST-pull down

Gtpbp2, *eEF1A1*, *Hbs1l*, and *eRF3α* coding sequences were cloned into pCMV-Tag4A (Life Technologies) to generate C-terminal FLAG-tagged proteins using primers indicated in table S2R. The Pelota and eRF1 coding sequences were HA-tagged at the C-terminus and cloned into pcDNA3. For co-immunoprecipitation, vectors were transiently transfected into HEK293T cells using Lipofectamine 2000 (Life Technologies). Immunoprecipitation was performed with mouse anti-M2 FLAG antibody (Sigma-Aldrich) pre-immobilized on Dynabeads (Life Technologies). Co-immunoprecipitated proteins were separated on SDS-PAGE gels, blotted, and detected by incubation with a mouse anti-HA antibody (Covance).

For GST-pull down assays, recombinant GST-fused *Gtpbp2*, *eEF1A1*, *Hbs1L*, and *eRF3α* were cloned in pGEX-4T2 (GE Healthcare Life Science), expressed in BL21(ED3) *E. coli*, and purified using glutathione-Sepharose 4B beads (Pfizer). Brains from 2-month-old wild type mice were homogenized in a buffer containing 20 mM Tris-HCl pH 7.4, 140 mM NaCl, 1% (v/v) Triton X-100 and supplemented with protease

inhibitors. The homogenate was centrifuged three times at 16,000 x g for 10 min, and the supernatant was incubated with recombinant protein bound to affinity beads. The resulting complexes were washed with 20 mM Tris-HCl pH 7.4, 140 mM NaCl, 0.1% (v/v) Triton X-100 and eluted by boiling in sample buffer. Membranes were probed with mouse anti-Pelota polyclonal antibodies (1:1000, Abnova).

For *in vitro* binding assays, the *Gtpbp2* coding sequence was cloned into pMALc4X vector (New England Biolabs), the *lacZα* gene of which was replaced with sequence encoding a histidine (His)-tag. Maltose-binding protein (MBP)-GTPBP2-His or MBP-His was purified with amylose resin. Full length Pelota was cloned into pGEX-4T2 (GE Healthcare Life Science), and GST-Pelota or GST alone was purified with glutathione resin. GST-Pelota or GST with MBP-GTPBP2-His or MBP-His was incubated with glutathione resin for 90 minutes in buffer (500 mM NaCl, 20 mM Tris-HCl pH 8.0, 3 mM βME, and 0.02% Triton X-100), followed by washing with the same buffer without Triton X-100. Pull down products was detected by western blot using a mouse antibody to Penta-His (Qiagen).

Ribosome profiling library construction

Mice were euthanized by cervical dislocation, and cerebella were immediately dissected out and frozen in liquid nitrogen within 30 seconds of euthanasia. Three cerebella were pooled from mice of each genotype for library generation. Tissue homogenization was performed with a mixer mill (Retsch MM400) in 1.0 ml of 20 mM Tris-Cl pH 7.4, 150 mM NaCl, 5 mM $MgCl_2$, 1 mM DTT, 1% (v/v) Triton X-100, 25 U/ml Turbo DNase I, 100 μg/ml cycloheximide, and 2 μg/ml harringtonine. RNase I-treated lysates were transferred to a 13 mm x 51 mm polycarbonate ultracentrifuge tube and 0.9 ml of a 1 M sucrose cushion was underlaid as previously described (*14*). Samples were ultracentrifuged in a TLA100.3 rotor at 70,000 r.p.m. at 4 °C for 4 hours to obtain the ribosome pellet. Pellets were then resuspended and RNA was extracted using the miRNeasy kit (Qiagen) according to the manufacturer's instructions. 26-nt to 34-nt RNA fragments were purified by electrophoresis on 15% polyacrylamide TBE-urea gel. Linker addition and cDNA generation and circularization were performed as previously described (*14*). Subtraction of rRNA with a pool of oligos was performed as described (*14*). Amplification of cDNAs was performed with previously described sets indexing primers to distinguish each sample (*14*) and the libraries were analyzed by sequencing on an Illumina HiSeq 2000 platform.

Read mapping

Material for each sample was split into two lanes for sequencing, yielding two fastq files that were then merged. Read mapping and quality control were performed computationally according to published protocols (*14, 15*). Read clipping and trimming were performed at the command line with options: 1) fastx_clipper -Q33 -a CTGTAGGCACCATCAAT -l 25 -c -n -v -i $fastqfile -o temp_clipped.fastq and 2) fastx_trimmer -Q33 -f 2 -l 100 -i temp_clipped.fastq -o temp_trimmed.fastq. Mouse ribosomal RNA sets were obtained by searching Genbank for known rRNAs and then filtering these out using the command: bowtie -p 16 rRNA temp_trimmed.fastq -l 23 --un temp_noRRNA.fastq > /dev/null. Reads with unique mapping to the mm10 genome were

computed using tophat and Illumina igenome annotations: tophat -p 16 -a 8 -m 0 -i 70 -I 500000 -g 1 --no-novel-juncs --library-type fr-firststrand –GTF /IlluminaGTF/Mus_musculus/UCSC/mm10/Annotation/Genes/genes.gtf /IlluminaGTF/Mus_musculus/UCSC/mm10/Sequence/BowtieIndex/genome/ temp_noRRNA.fastq. Manual inspection of coding loci with high read counts also revealed an additional rRNA overlapping a coding region, which was removed from consideration in further data analysis (LSU-rRNA_Hsa, on mm10 chr6). The total reads were between 44 and 58 million for each sample and 5.6 to 8.0 million of these reads uniquely mapped to CDS regions. Data are summarized in table S2S.

Positioning of reads with respect to the ribosome

We initially assumed that the center of reads would overlap the codon in the P site of the ribosome. Using this assumption we found a strong excess of reads near AGA codons, such that the center of the read mapped one codon upstream of the AGA codon (fig. S10). This would correspond to pausing when the AGA would be in the ribosomal A site, which is consistent with the paucity of $tRNA^{Arg}_{UCU}$ due to the *n-Tr20* mutation. For this positioning rule, we in general rounded up, i.e. if the read were 26-27 nt long, we added a count at the position where the 14^{th} nt of the read mapped; 28-29 nt long added a count at the mapped position of the 15^{th} nt of the read; 30-31 nt long at the mapped position of the 16^{th} nt of the read, etc. This "read center" rule for determining the codon in the ribosomal P site was also consistent with behavior at the stop codon, as we observed an increase in footprinting reads when the ribosomal A site was inferred to overlap a stop codon.

However, during manual inspection we found that the quality of inference of ribosome position varied significantly as a function of read length and the codon frame in which the read mapped. This is likely because of length-specific biases in the positions at which mRNA would be digested with respect to the ribosome boundaries. So we assumed that for all read lengths the ribosome would be predominantly located in one position relative to the AGA. While the majority of our sequence reads were 27-29 nts as expected (*15*), inspection of a number of transcripts from several genes indicated that, as previously reported (*22*), RNase cleavage was not always complete with more variable digestion on the 3' side of the ribosome often resulting in additional nucleotides on the 3' end of the sequence reads. We therefore adjusted our positioning rule so that the codon assumed to be in the ribosome P site would always be one of the two codons closest to the center of the read. Out of these two codons, we chose the one such that the length of sequence 5' of the P site would be ≤ the length of sequence 3' of the P site. This rule substantially improved the AGA signal so we adopted it for all subsequent analysis (fig. S10). In practice, this means the P site is remapped by the rules described in the following pseudocode:

```
# $pos is the position of the center of the read. Rounded up for reads with an even number of nt.
# $readlen is the length of the read.
# $posframe is the codonframe of the center of the read, as defined above.
# $lenrem is the length of the read modulo 6.

  $posframe = $pos % 3;
```

```
$lenrem = $readlen % 6;

# Function to calculate $offset.

#length 26
if (($posframe == 2) && ($lenrem == 2)) {return -3;}
if (($posframe == 0) && ($lenrem == 2)) {return -1;}
if (($posframe == 1) && ($lenrem == 2)) {return -2;}

#length 27
if (($posframe == 2) && ($lenrem == 3)) {return 0;}
if (($posframe == 0) && ($lenrem == 3)) {return -1;}
if (($posframe == 1) && ($lenrem == 3)) {return -2;}

#length 28
if (($posframe == 0) && ($lenrem == 4)) {return -1;}
if (($posframe == 1) && ($lenrem == 4)) {return -2;}
if (($posframe == 2) && ($lenrem == 4)) {return -3;}

#length 29
if (($posframe == 0) && ($lenrem == 5)) {return -1;}
if (($posframe == 1) && ($lenrem == 5)) {return -2;}
if (($posframe == 2) && ($lenrem == 5)) {return 0;}

#length 30
if (($posframe == 1) && ($lenrem == 0)) {return -2;}
if (($posframe == 2) && ($lenrem == 0)) {return -3;}
if (($posframe == 0) && ($lenrem == 0)) {return -1;}

#length 31 or length 25
if (($posframe == 1) && ($lenrem == 1)) {return -2;}
if (($posframe == 2) && ($lenrem == 1)) {return 0;}
if (($posframe == 0) && ($lenrem == 1)) {return -1;}

$newpos = $pos + $offset;

# $newpos is the corrected position. This position is assumed to be at the 2nd codon position of the codon overlapping the ribosomal P site.
```

Footprint RPKM values (fig. S11) were calculated by considering all reads on the coding exons of each gene. Mapped reads were visualized on Integrative Genomics Viewer (IGV browser, version 2.3 for Mac, https://www.broadinstitute.org/software/igv/download). Images were screen captured and footprints in which the AGA codon was in the A site were identified manually (fig. S16).

Average pausing around codons

To determine the average pausing behavior around a codon, e.g. AGA (Fig. 4F), we first identified all instances of that codon in CDS regions. To do this, mm10 CDS sequences for each transcript were downloaded from the UCSC genome browser based on their RefGene IDs. Error-checking revealed a small number of sequences with lengths not divisible by three and these were removed from further analysis. Codons were then identified in each of these CDS sequences. To avoid double counting of codons, we only used one transcript for each gene, with genes defined by all transcripts with a common start codon location. The selected transcript was the one with the 3' most stop codon. For each codon *c* (e.g. *c=AGA*) we calculated the counts of reads mapped to positions at all instances of *c*. For each position *p* up to three codons in either direction we also calculated the number of reads mapping there (i.e. $p \in [-3,3]$). Reads were added together on a codon basis, rather than on a nucleotide level. The values of Reads(*c*, *p*) were summed across all instances of *c* to yield an observed value for Total Reads(*c,p*).

To determine the expected value for Total Reads(*c,p*), we used a null model in which the number of reads on any transcript was held constant but the locations of reads were randomized, i.e. at any given codon the expected number of reads would be 3*(# reads on transcript)/length of transcript. This value was summed on a transcript-specific basis for all instances of codon *c* to yield Expected Total Reads(*c,p*). Note that this null model results in an expected value independent of the position *p*. The values reported in Fig. 4F are the Total Reads(*c,p*)/Expected Total Reads(*c,p*).

Pause site identification

To identify pause sites, we looked for excess reads at an individual codon compared to the background. In principle, this background should be determined by the average reads per codon in the transcript. However, we observed that because of splice isoforms, some transcripts have blocks of codons with read levels significantly elevated above the transcript-level background. To correct for this, we implemented a procedure to identify pause sites with read levels above both the transcript-wide background and their local context. For the transcript-wide background, we defined $BG_{transcript}$ = average footprints per codon in the first 150 codons of the CDS (or the whole transcript if its length was less than 150 codons). This rule was chosen to be consistent with prior literature (*23*). $BG_{transcript}$ is the quantity that was used for analysis of reads per codon on transcripts (figs. S12-S14, and S16).

The local context of reads was also calculated to eliminate false positive pausing sites due to potential alternative splicing events. Alternative splice events can create a plateau of elevated read counts if there is an unannotated exon. To avoid counting such sites as pauses we required pauses to have higher counts than the local context. To determine the local context, we tabulated footprint counts in each of the 3 codons immediately left of a site, calculated the median of these 3 values, and divided by 3 to get the counts per nucleotide on the left, defining a quantity BG_{left}. We did the same thing for the 3 codons immediately right of a site to define the quantity BG_{right}. We then set BG = MAX($BG_{transcript}$, BG_{left}, BG_{right}).

For each codon in all CDS sequences, we calculated a pause strength P based on a z-score-like quantity: P= (observed reads – BG) / $(BG)^{1/2}$. Here we have assumed a standard deviation $(BG)^{1/2}$ as would be expected under Poisson noise. In most analyses, pause sites were thresholded at P≥10. In a z-score model, the probability of having P≥10 at a specific codon is <1e-20. At this threshold for detecting pauses, we would expect far less than one false positive in the entire mouse transcriptome (~10^7 codons). We chose this stringent threshold to buffer us from the approximate nature of the Poisson null model.

Note that if background levels were too low then codons having even a single footprint would be spuriously classified as being a pause site. For example, at BG=0.01, we have P=9.9 when there is just one read at a codon, very nearly meeting the pause strength threshold. To avoid this problem, we only searched for pauses in genes with average footprints/codon > 0.1 (i.e. $BG_{transcript} > 0.1$) (figs. S11 to S14). Under this background model and assuming z-score statistics, for a codon with a single read we would have P=(1-0.1)/sqrt(0.1) = 2.8, which is far below the P≥10 threshold of classifying a pause site. As an example, for a transcript with 0.1 reads per codon, at least 4 reads are necessary on a given codon for it to meet the P=10 threshold (i.e. (4-0.1)/sqrt(0.1) > 10, but (3-0.1)/sqrt(0.1) < 10). We also compared pause strength across replicates at various thresholds for the footprints/codon level (fig. S14). We observed significant concordance in pause scores at this 0.1 reads per codon threshold, and this threshold still allowed us to consider ~10000 transcripts in each experiment (fig. S13).

Codon Usage at Pause Sites

The calculations of codon usage at pause sites and background codon usage (Fig. 4G) were performed as follows. For the background codon usage, we counted all the codons in each gene with at least 0.1 footprints per nucleotide. To avoid double counting of codons, we only used one transcript for each gene, with genes defined by all transcripts with a common start codon location. The selected transcript was the one with the 3'most stop codon. Using these codons, we determined the fraction of each type of codon $f^{background}(codon)$. These fractions were normalized based on all 61 translated + 3 stop codons such that summing over the 64 codons gives $\sum_{codons} f^{background}(codon) =$. We performed an analogous calculation to determine codon usage at pause sites. Here we used the same dataset as for the background calculation but restricted to codons with a pause strength P≥10.

Comparison of pause sites across biological replicates

To determine whether AGA pause sites were robust across biological replicates (table S4), we examined whether genes containing AGA pauses were similar across replicates. For replicates, mice of the same age were used, and samples were harvested and libraries were generated on different days. For this comparison, we used a null model in which genes were treated equally. The list of possible genes was restricted to those with > 0.1 reads/codon and only genes having at least one AGA. Let N_1 be the number of genes meeting this criterion in replicate 1 and N_2 be the number of genes meeting this criterion in replicate 2. Let X_1 be the number of genes with a pause in replicate 1 and let X_2 be the number of genes with a pause in replicate 2. Then if pause sites were random, the

expected number of genes overlapping in the two replicates would be: Expected = X_1 X_2 min(N_1, N_2) / (N_1 N_2).

We also calculated whether AGA pauses within each transcript tended to overlap between replicates. Because genes with small numbers of AGA sites are more likely to have overlapping pauses, we implemented a procedure that corrects for this bias. As our null model, in each replicate we shuffled pausing strengths among AGA codons within each transcript, considering only those AGA sites with at least one read. This procedure was performed 100 times, and the mean and standard deviation of the overlap in these shuffled controls were used to calculate a z-score for the excess overlap of the actual data.

Gene ontology

The gene lists of transcripts with P≥10 ribosome stalls in B6J-*nmf205*$^{-/-}$ cerebellar libraries were uploaded into Gene Ontology (GO) and analysis was performed using the DAVID bioinformatics web server (http://david.abcc.ncifcrf.gov/) (*24*). The functional annotation chart and clustering analysis modules were employed for gene-term enrichment analysis and the background was set to the "Mus musculus" option available in DAVID. In table S2Q, we show both the EASE score implemented in DAVID, which is a modified Fisher Exact *p*-value, and the Benjamini *p*-value that is one of the multiple testing correction techniques and is a set as default in DAVID, for GO terms in which the uncorrected *p*-Value (the EASE score) of one or more members of an annotation cluster is $<1x10^{-5}$.

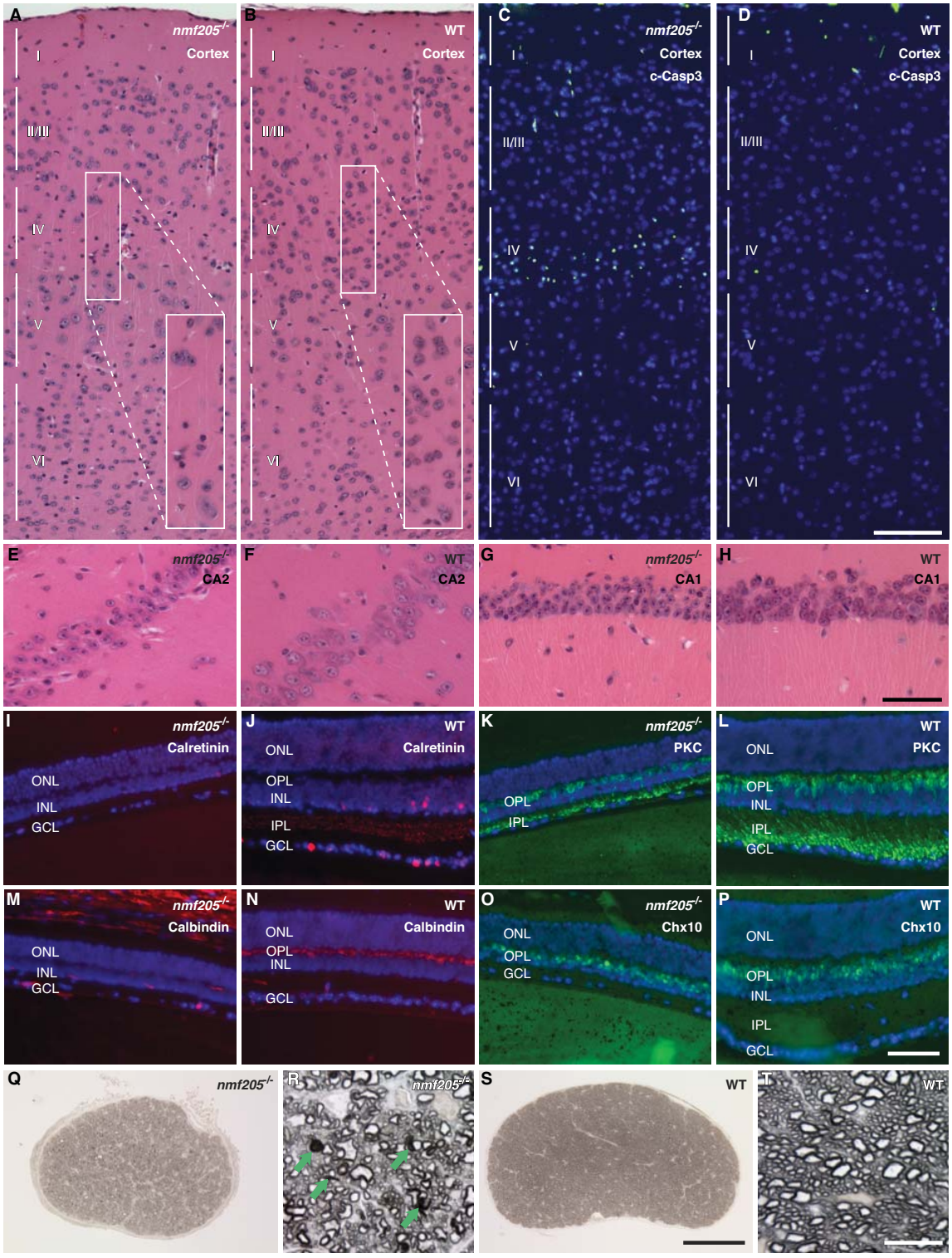
A
nmf205-/-
Cortex
I
II/III
IV
V
VI
B
WT
Cortex
C
nmf205-/-
Cortex
c-Casp3
D
WT
Cortex
c-Casp3
E
nmf205-/-
CA2
F
WT
CA2
G
nmf205-/-
CA1
H
WT
CA1
I
nmf205-/-
Calretinin
ONL
INL
GCL
J
WT
Calretinin
OPL
IPL
K
nmf205-/-
PKC
L
WT
PKC
M
nmf205-/-
Calbindin
N
WT
Calbindin
O
nmf205-/-
Chx10
P
WT
Chx10
Q
nmf205-/-
R
S
WT
T

Fig. S1. Progressive neurodegeneration in the *nmf205*$^{-/-}$ mouse.
(**A** and **B**) Hematoxylin and eosin-stained sagittal sections of wild-type (WT; +/+) and B6J-*nmf205*$^{-/-}$ cortex. Cortical layers are indicated, and a higher magnification image of the boxed region in layer 4 is shown as an insert. (**C** and **D**) Immunohistochemistry with anti-cleaved caspase 3 antibody (c-Casp3) on sections of cortex (green). Sections were counterstained with Hoechst 33342 (blue). (**E** to **H**) Sagittal sections of wild type and B6J-*nmf205*$^{-/-}$ hippocampal CA2 (**E** and **F**), and CA1 (**G** and **H**) regions were stained with hematoxylin and eosin. Note the increase in pyknotic nuclei in pyramidal neurons found in the CA2, but not CA1, region of the hippocampus of mutant mice. (**I** to **P**) Immunofluorescence was performed on cross sections of WT and B6J-*nmf205*$^{-/-}$ retina with antibodies to calretinin to visualize amacrine cells (**I** and **J**), protein kinase C (PKC) to visualize bipolar cells (**K** and **L**), calbindin D-28 to visualize horizontal cells (**M** and **N**), and Chx10 to visualize bipolar cells (**O** and **P**). Sections were counterstained with Hoechst 33342. (**Q** to **T**) Cross sections of B6J-*nmf205*$^{-/-}$ and WT optic nerves stained with *p*-phenylenediamine. Degenerating axons are marked with arrows in the higher magnification images of B6J-*nmf205*$^{-/-}$ optic nerve (**R**). All sections were from 2-month-old mice except for those in (**C** and **D**) that were from 5-week-old mice. ONL, outer nuclear layer; OPL, outer plexiform layer; INL, inner nuclear layer; IPL, inner plexiform layer; GCL, ganglion cell layer. Scale bars, 100 μm (**D** and **S**), 50 μm (**H** and **P**), and 2 μm (**T**).

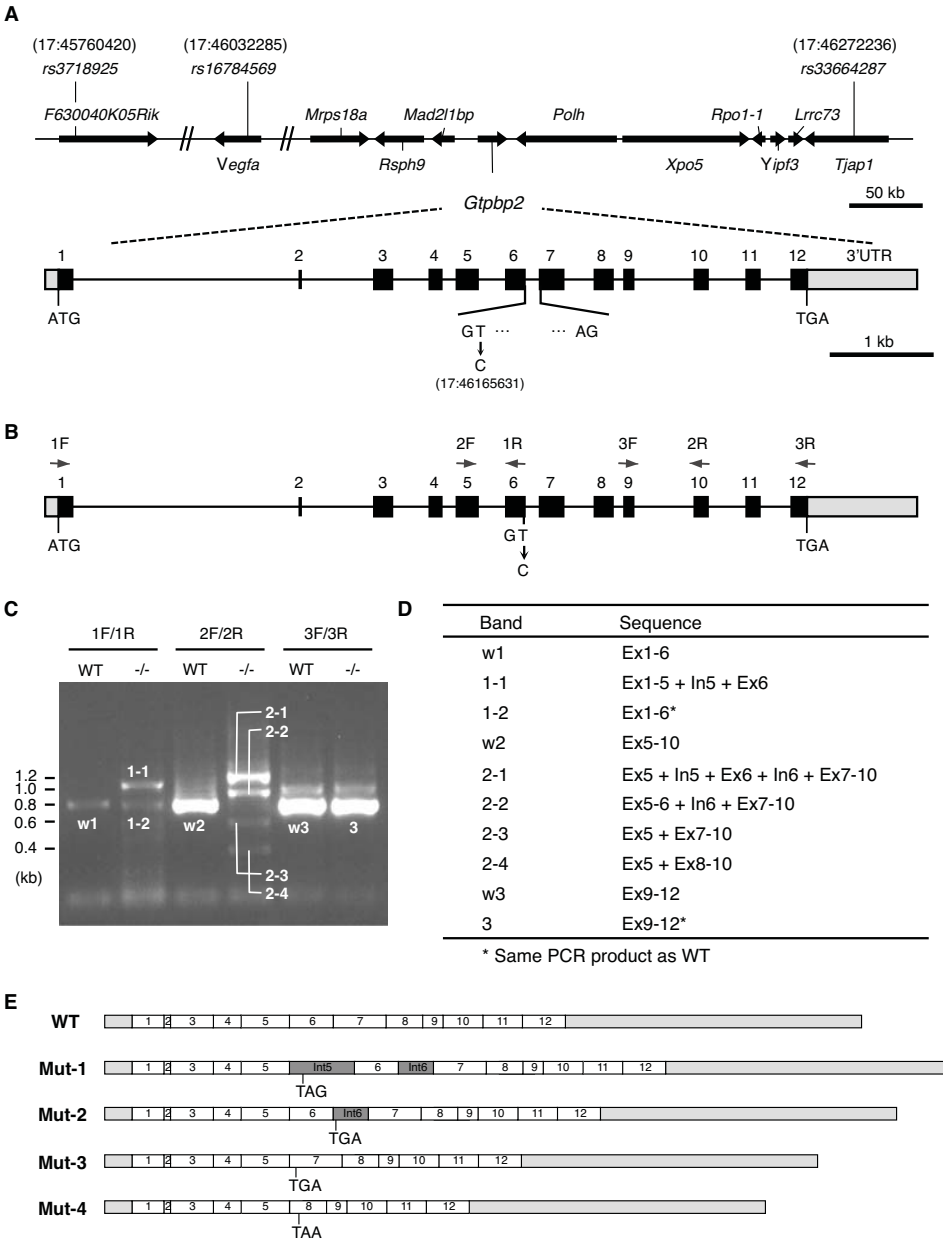

Fig. S2. The *nmf205* mutation causes abnormal splicing of *Gtpbp2* transcripts. (**A**) The *nmf205* critical interval showing the location of the mutation in the splice donor site of intron 6 of *Gtpbp2* gene. Chromosome positions are from the GRCm38 assembly. Exons and UTRs are indicated by black and gray boxes, respectively. (**B**) Arrows indicate the location of primers (see table S2R) used for RT-PCR. (**C**) *Gtpbp2* splicing abnormalities in the B6J-*nmf205* mutant brain. PCR was performed using oligo-dT primed cDNAs generated from wild-type (WT, +/+) and *nmf205*$^{-/-}$ (-/-) brain mRNAs and RT-PCR products were separated by agarose gel electrophoresis. (**D**) Identification of PCR products based on sequencing results. (**E**) Schematic of *Gtpbp2* isoforms in the *nmf205*$^{-/-}$ brain. Note that all of the mutant transcript isoforms have premature stop codons.

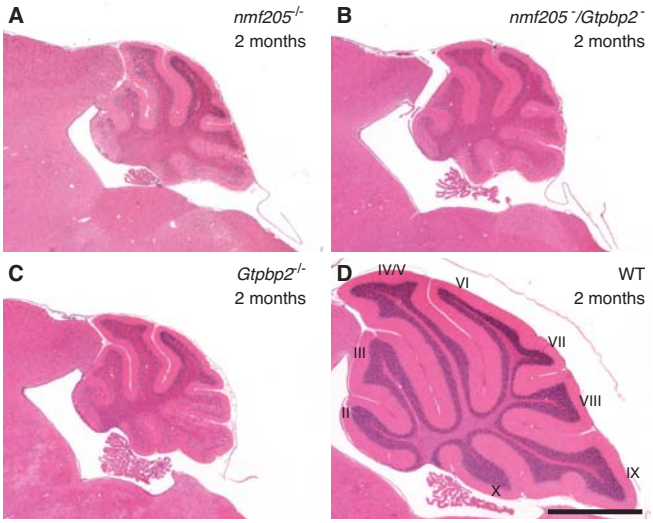

Fig. S3. Loss of *Gtpbp2* is causative for neurodegeneration in B6J-*nmf205*$^{-/-}$ mice. A genetic complementation test confirms loss of *Gtpbp2* is causative for neurodegeneration in B6J-*nmf205* mutant mice as shown by hematoxylin and eosin-stained sagittal sections of cerebella from 2-month-old B6J-*nmf205*$^{-/-}$(**A**), B6J-*nmf205*$^{-}$ */Gtpbp2*$^{-}$ (**B**), B6J-*Gtpbp2*$^{-/-}$(**C**), and wild-type **(**WT; **D**) mice. Cerebellar lobules are indicated by Roman numerals. Scale bar, 1 mm.

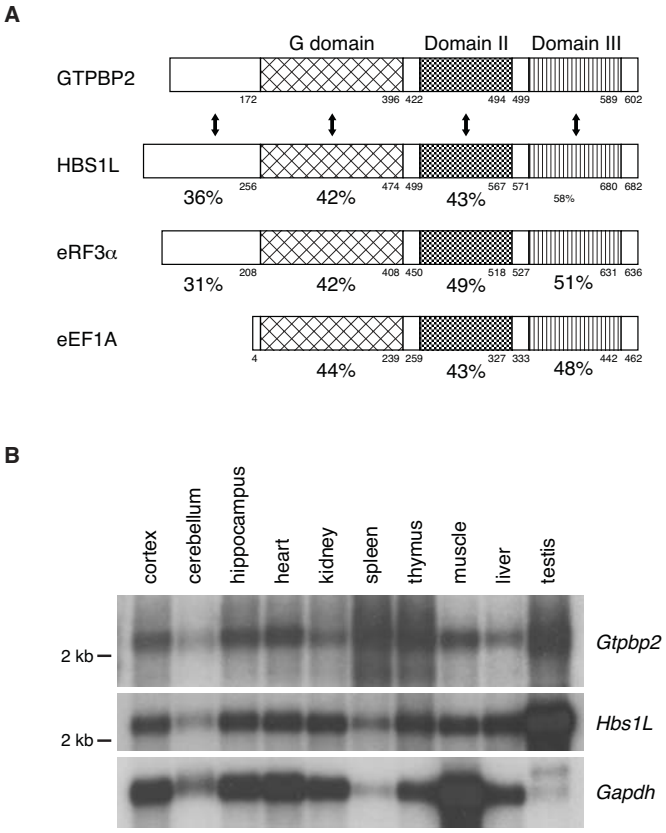

Fig. S4. Domain structure and expression of *Gtpbp2* and *Hbs1l*.
(**A**) Amino acids at the domain boundaries are numbered and the percent homology of these domains and the N-terminus of mouse GTPBP2 with mouse HBS1L, eRF3α, and eEF1A proteins are indicated. (**B**) Northern blot analysis of *Gtpbp2* and *Hbs1L* in various mouse tissues.

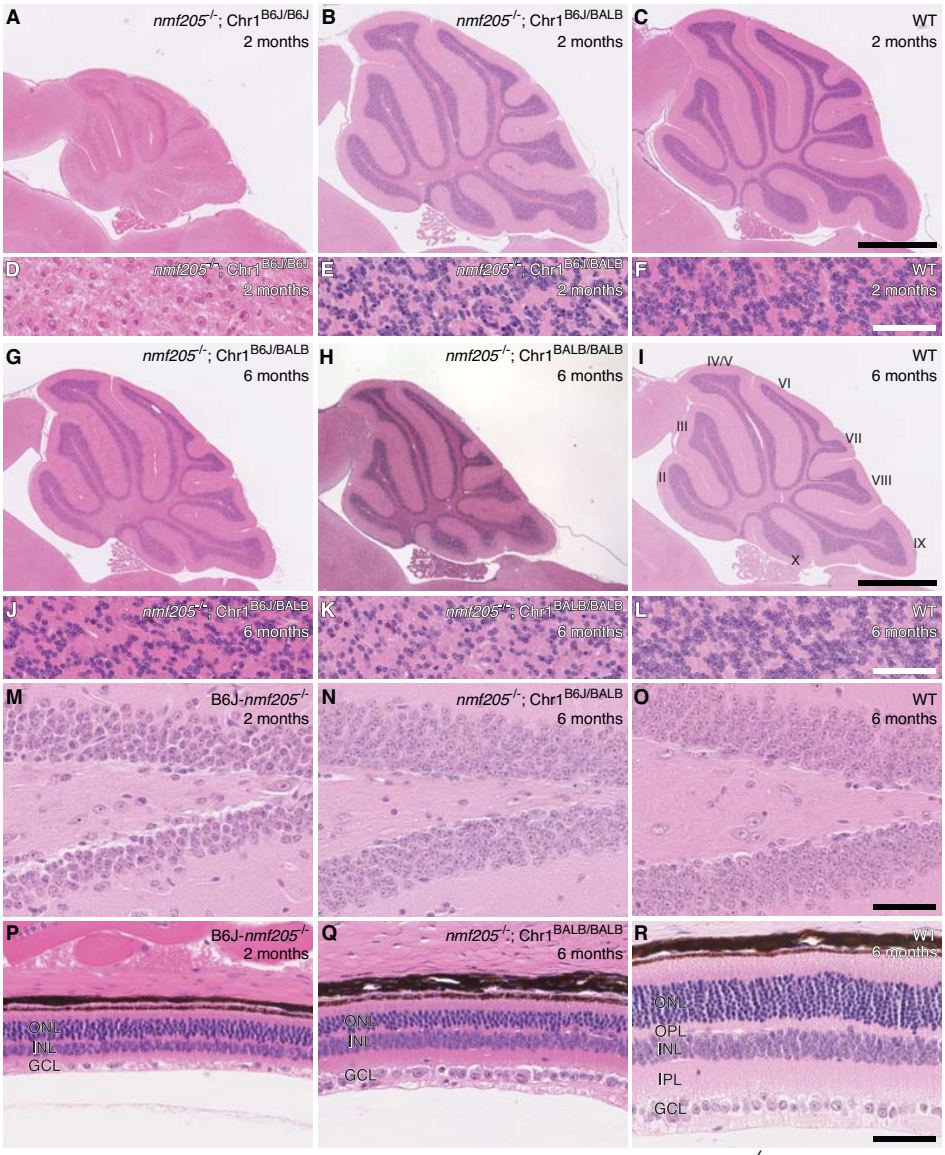

Fig. S5. Congenic rescue of neurodegeneration in the *nmf205*$^{-/-}$ mice.
(**A** to **C**) Hematoxylin and eosin-stained sagittal sections of cerebella from 2-month-old *nmf205*$^{-/-}$ mice that were homozygous for B6J alleles on Chromosome 1 (Chr1$^{B6J/B6J}$) (**A**), *nmf205*$^{-/-}$; B6J.BALB$^{Chr1(B6J/BALB)}$ (Chr1$^{B6J/BALB}$) mice (**B**), and wild-type (WT, B6J) mice (**C**). (**D** to **F**) Higher magnification images of lobule IX from (**A** to **C**). (**G** to **I**) Hematoxylin and eosin-stained sagittal sections of cerebella from 6-month-old *nmf205*$^{-/-}$; Chr1$^{B6J/BALB}$ (**G**) *nmf205*$^{-/-}$; B6J.BALB$^{Chr1(BALB/BALB)}$ (**H**) and B6J mice (**I**). (**J** to **L**) Higher magnification images of lobule IX from (**G** to **I**). (**M** to **O**) Hematoxylin and eosin-stained sagittal sections of the dentate gyrus from 2-month-old B6J-*nmf205*$^{-/-}$ (**M**), 6-month-old *nmf205*$^{-/-}$; Chr1$^{B6J/BALB}$ (**N**) and 6-month-old B6J mice (**O**). (**P** to **R**) Hematoxylin and eosin-stained sagittal sections of the retina from 2-month-old B6J-*nmf205*$^{-/-}$ (**P**), 6-month-old *nmf205*$^{-/-}$; Chr1$^{BALB/BALB}$ (**Q**) and 6-month-old B6J mice (**R**). ONL, outer nuclear layer; OPL, outer plexiform layer; INL, inner nuclear layer; IPL, inner plexiform layer; GCL, ganglion cell layer. Scale bars, 1 mm (**C** and **I**), 50 μm (**F**, **L**, **O**, and **R**).

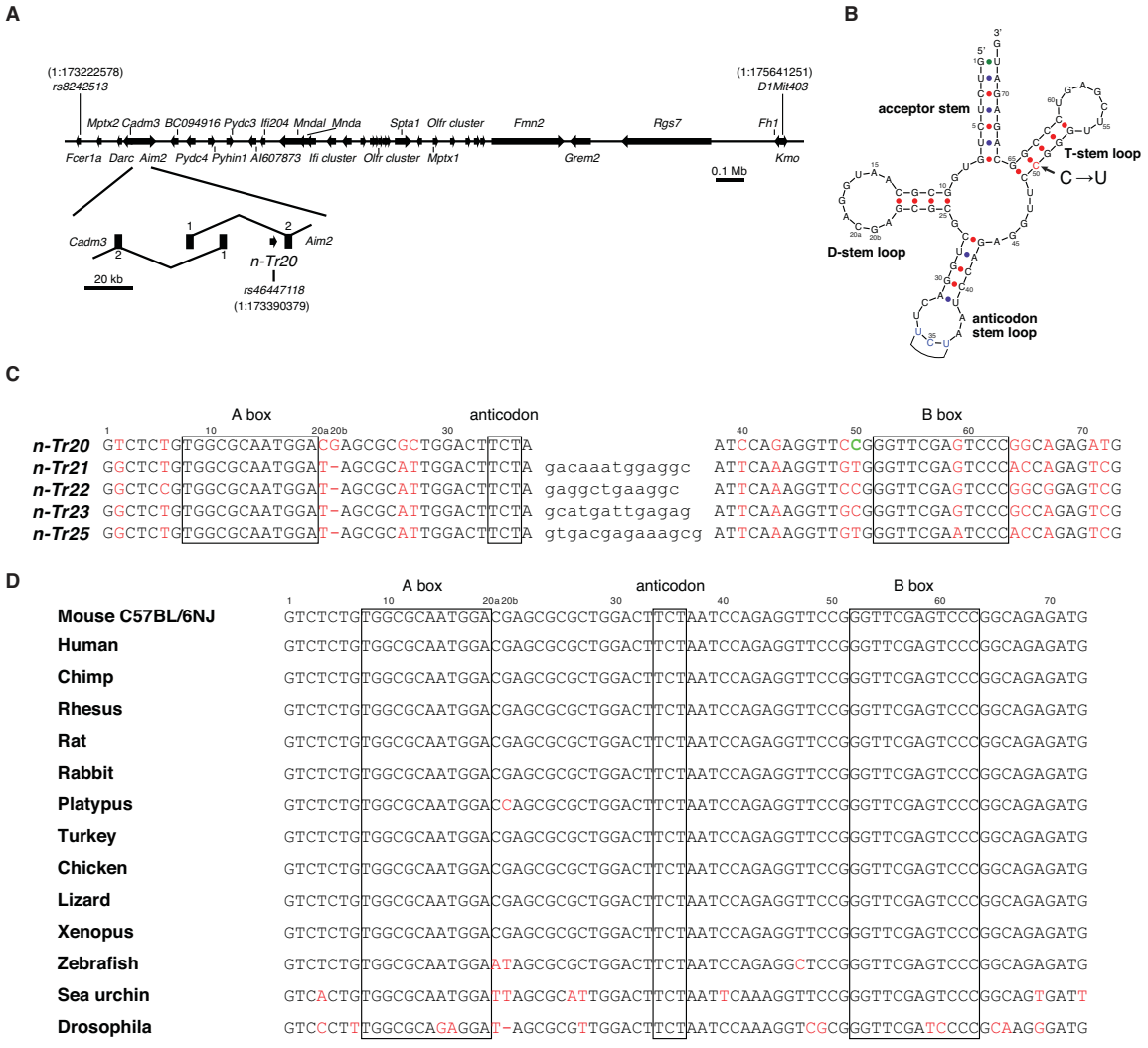

Fig. S6. *Mod205* is a mouse tRNA$^{Arg}_{UCU}$ gene.
(**A**) The *Mod205* critical region showing the location of *rs46447118* in the tRNA$^{Arg}_{UCU}$ gene, *n-Tr20*. Chromosome positions are assigned according to the GRCm38 assembly. (**B**) mFold (http://mfold.rna.albany.edu/?q=mfold) prediction of the secondary structure of wild-type *n-Tr20* tRNA$^{Arg}_{UCU}$. Predicted base pairs are indicated by red (G-C), blue (A-U) and green (G-U) dots. (**C**) The sequence of the mouse tRNA$^{Arg}_{UCU}$ isodecoders is shown. Introns are in lower case, the C50T mutation is shown in green, and SNPs between isodecoders are highlighted in red. The anticodon and the dual A and B box internal promoters are boxed. (**D**) Sequence alignment of putative *n-Tr20* orthologs in several vertebrate and invertebrate species.

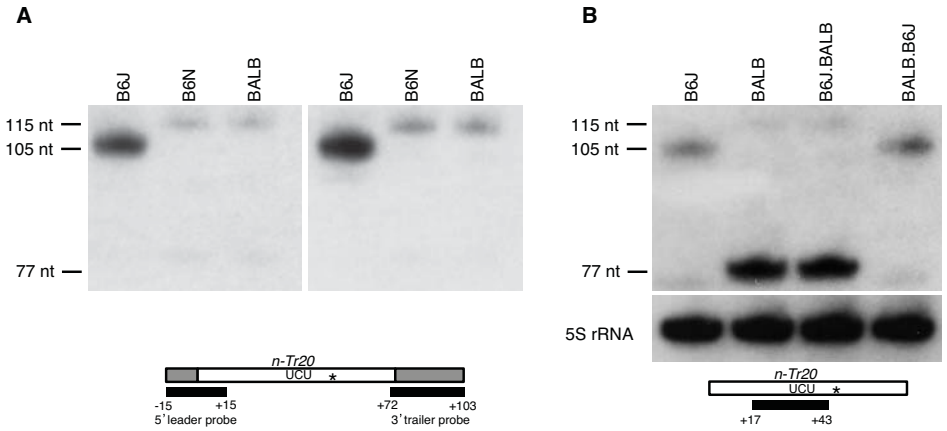

Fig. S7. The B6J genome is responsible for abnormal processing of *n-Tr20*.
(**A**) Northern blot analysis of brain RNA from P30 B6J, B6N and BALB/cJ mice. The blot shown in Fig. 3B was stripped and reprobed using the oligonucleotides indicated by the solid black lines on the schematic (see table S2R). Autoradiographs of the blot hybridized with a probe to the 5' leader or the 3' trailer of *n-Tr20* are shown on the left and the right, respectively. The asterisk in the schematic indicates the mutation site. (**B**) Northern blot analysis of brain RNA from P30 B6J, BALB, B6J.BALB$^{Chr1(BALB/BALB)}$ (B6J.BALB) and BALB.B6J $^{Chr1(B6J/B6J)}$ (BALB.B6J) mice. The position of the probe used for hybridization is indicated by a solid black line on the schematic. 5S rRNA hybridization is shown as a loading control for this figure.

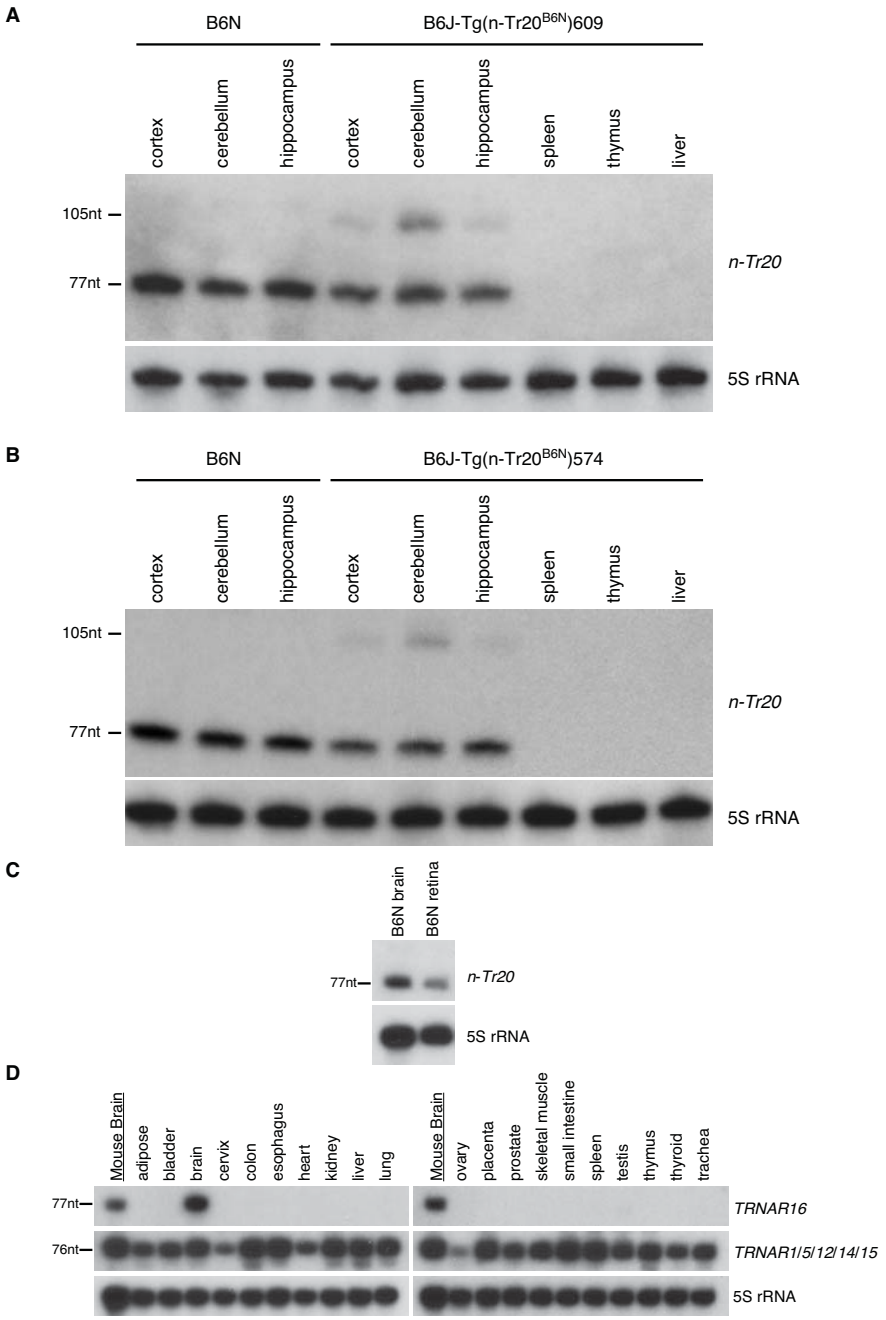

Fig. S8. Expression of *n-Tr20* and its human ortholog, *TRNAR16*.
(**A** and **B**) Northern blot analysis of *n-Tr20* expression in P30 mice in the B6J-Tg(n-Tr20^{B6N}) transgenic lines Tg609 (**A**) and Tg574 (**B**). Note the brain-specific expression. Blots were hybridized with the internal *n-Tr20* probe shown in fig. S7B. (**C**) Northern blot analysis of *n-Tr20* in brain and retina from P30 B6N mice using the same probe as **(A)**. (**D**) Northern blot analysis of the human *n-Tr20* ortholog, *TRNAR16*, (upper panel) and its isodecoders (middle panel). Mouse brain RNA is loaded as a control. 5S rRNA was used as a loading control.

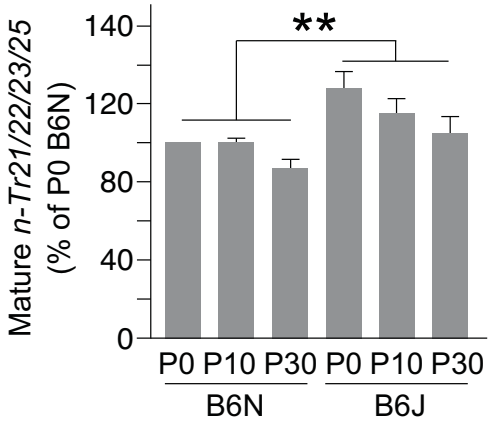

Fig. S9. Expression of *n-Tr21/22/23/25* in B6N and B6J brains.
Graph showing densitometric analysis of northern blots of B6N and B6J brains (n=4) probed with an oligonucleotide probe complementary to *n-Tr21/22/23/25* $tRNA^{Arg}_{UCU}$ (see table S2R). Error bars indicate SEMs. $^{**}P < 0.005$.

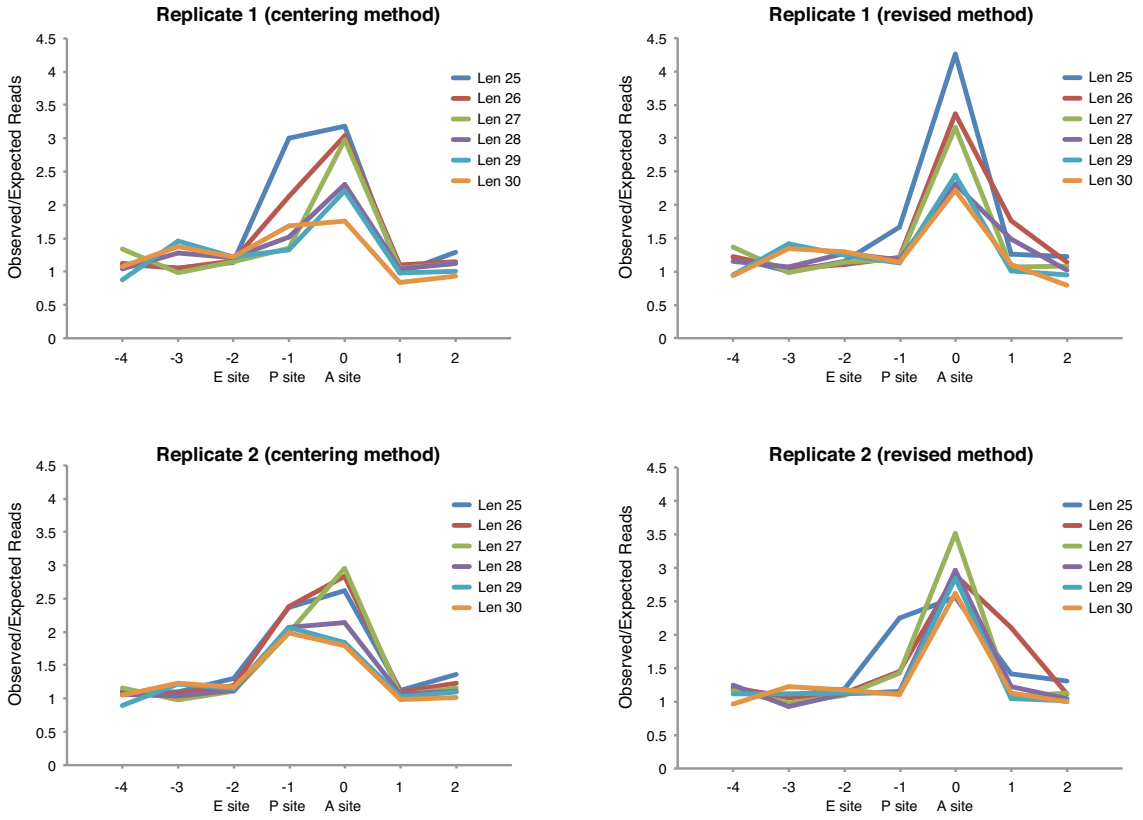

Fig. S10. Improvements in ribosome footprint mapping based on read length. Both ribosomal footprinting replicates from the B6J-*nmf205*$^{-/-}$ cerebellum were analyzed as shown. We considered the behavior of positional assignment as a function of read length, since most reads in our study were 25-30 nts, with a median read length of 28-29 nts in all experiments. We initially considered a positioning method in which we assumed the center of each read would be at the ribosomal P site (left side of figure). Note that the precision of positioning of reads (as indicated by the sharpness of the peak with AGA assigned to the ribosomal A site) varied as a function of read length, with the sharpest peaks observed for read lengths 27-29. Moreover, in replicate 2 (bottom left) we observed that for reads of length 30, the peak did not even occur at the A site. We therefore tested a revised positioning method taking into account the read length and the codon frame of the center of the aligned read, as described in the Methods. Using this revised method, a more strongly peaked signal was observed (right side of figure). This procedure narrowed the width of the peak from approximately 2 codons to approximately 1 codon and also caused the peaks to line up at the A site for every read length in both replicates. All graphs describe observed/expected reads at ribosomal positions near AGA codons.

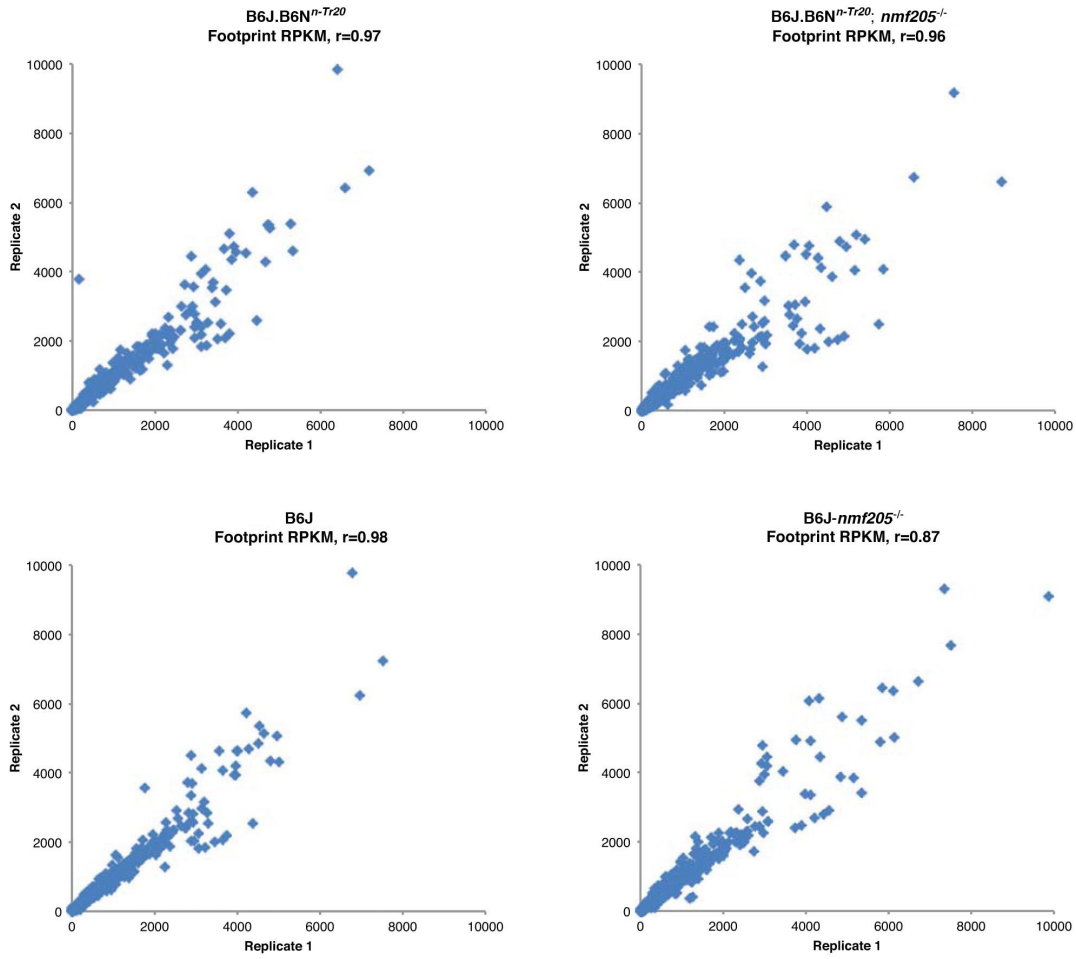

Fig S11. Correlation of ribosome footprinting RPKM values across replicates. Plots show CDS footprinting RPKM values across biological replicates for transcripts using mm10 mouse annotations. All strains show strong correlations across replicates, with Pearson correlations ranging from 0.87-0.98.

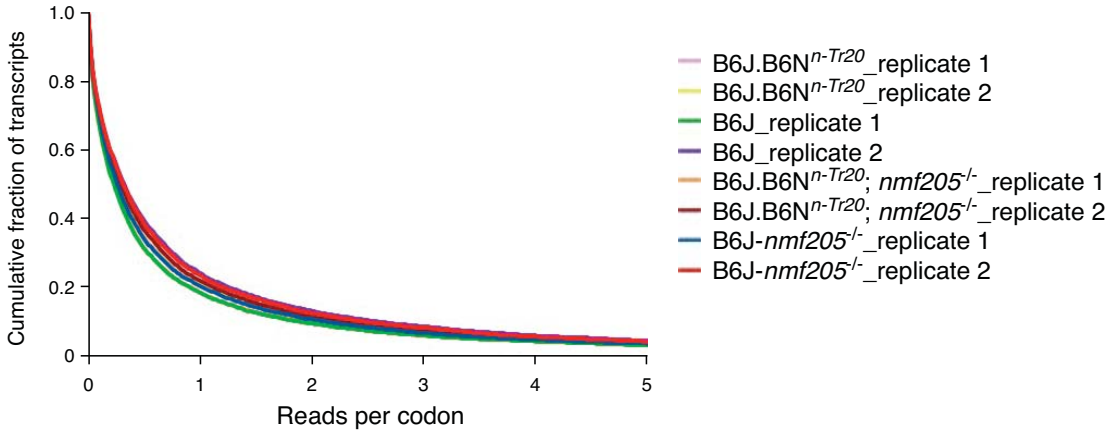

Fig. S12. Cumulative distribution of footprint reads per codon, a measure of read density for each transcript. For each genotype, two biological replicates are shown. These distributions are over the transcripts that have at least 1 footprint read in each respective experiment. The numbers of such transcripts range from 15563-16146 across the 8 experiments. As a threshold for inclusion for further analysis of pause sites, we consider only transcripts with at least 0.1 reads per codon in the first 150 codons of the transcript, as described in the Methods. At this threshold, there are ~10000 transcripts in each experiment (see also fig. S13).

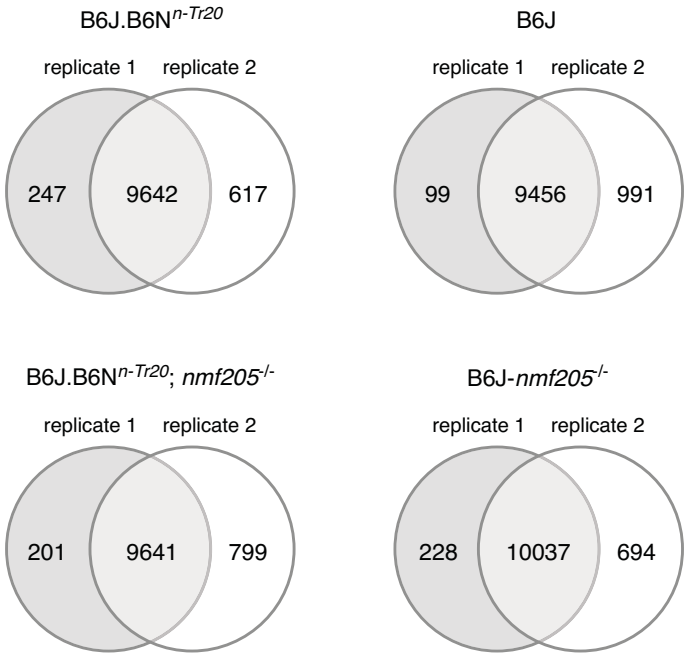

Fig. S13. Reproducibility of number of genes meeting inclusion criteria.
For each genotype in the ribosome pausing analysis, Venn diagrams show the number of genes meeting the read coverage threshold (set as 0.1 footprint reads/codon) as well as the intersection between the two biological replicates. As the total number of annotated genes before exclusion is 20,324, about half of annotated genes are assigned pause scores (P) along their transcripts and thus included in our ribosome pausing analysis.

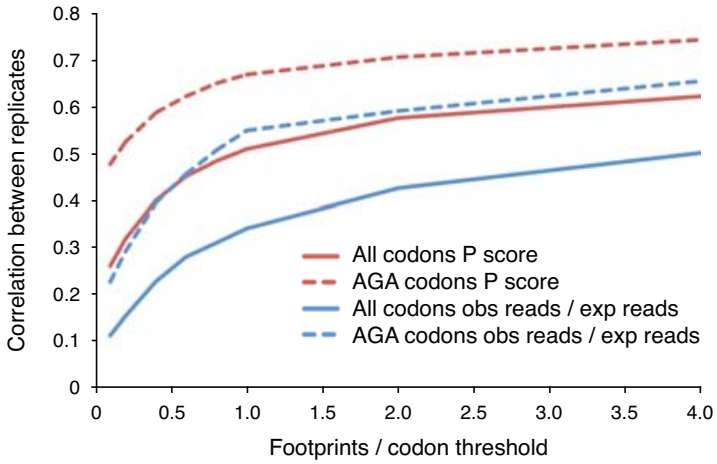

Fig. S14. Correlation of ribosome pausing between biological replicates.
The Pearson correlation of P scores between biological replicates is shown for all codons (red lines) or just AGA codons (dashed red lines), where only transcripts with a minimum footprint reads/codon threshold in both replicates are considered. We observe significant correlations even at the 0.1 footprints/codon threshold (r=0.26 for all codons; r=0.48 for AGA codons). Correlations further increase when restricting to transcripts with higher footprint densities. When (observed/expected reads) is used to assess pausing at each codon instead of P score, correlations are weaker (blue solid and dashed lines. At the 0.1 footprints/codon threshold r=0.11 for all codons; r=0.23 for AGA codons). This illustrates the greater susceptibility of raw read counts to stochasticity, in comparison to P scores. The *p*-values of all Pearson correlations are <1e-200.

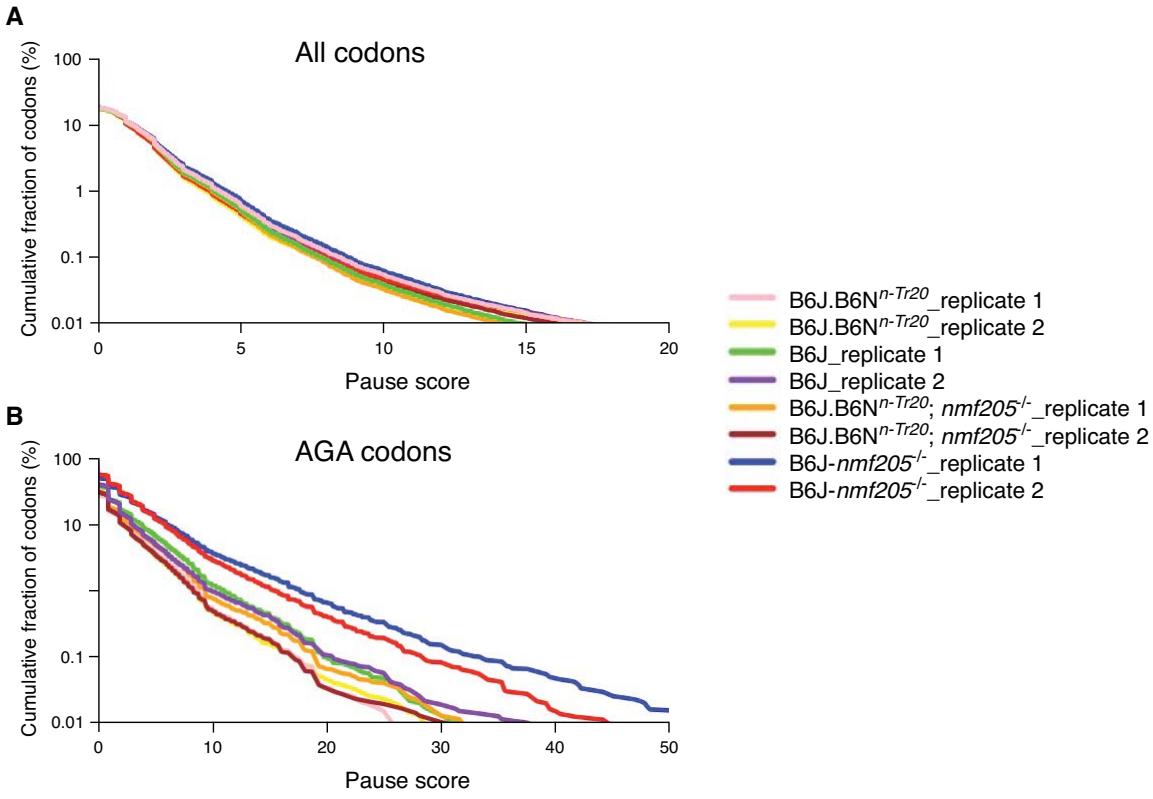

Fig. S15. Distribution of P scores in individual replicates.
Cumulative distribution of pause scores at all codons (**A**), and AGA codons only (**B**) in the four strains analyzed. For each strain, data from each biological replicate is plotted. Note that there are a large number of codons with pause score equal to zero. So all curves have a discontinuous jump in value to 100% at P=0.

Fig. S16. Examples of reads at AGA pauses.
IGV (Broad Institute) browser images from twelve representative genes with (P≥10) AGA pauses in B6J-*nmf205*$^{-/-}$ cerebellum. Images show data from replicate 1 for each strain in genes with a wide range of P values (10.3-45.0) and a range of footprint reads per codon (0.41-6.87). The AGA codon is bracketed by red vertical lines, and footprints in which the AGA codon was in the A site are shown in red. For each panel, the gene name, the pause location, the pause score (P), and the footprint reads per codon are shown. Genes with lower P scores (e.g. *Lin7c*) or lower footprint reads per codon (e.g. *Hivep2*) also show significant accumulation of AGA reads in B6J-*nmf205*$^{-/-}$ cerebella. The *Zfp238* pause shown here (codon 492) is marked by an asterisk in Fig. 4E.

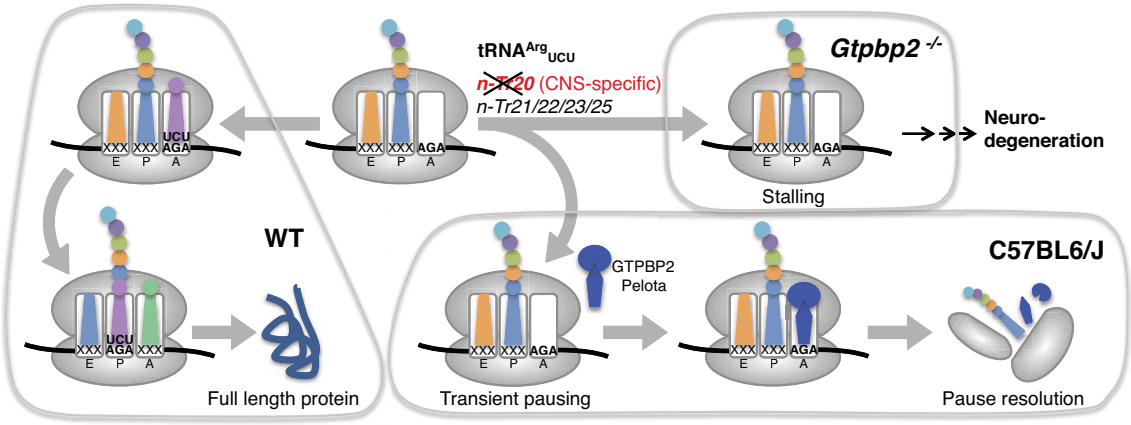

Fig. S17. A working model of GTPBP2 and tRNA deficiency.
The reduction in the pool of tRNA$^{Arg}_{UCU}$ in B6J brain leads to an increase in ribosome pausing at AGA codons during elongation that is largely resolved by GTPBP2:Pelota. In the absence of GTPBP2, ribosome stalling at AGA codons is increased, leading to neurodegeneration.

Strain used for F2 cross	Number of affected mice / *nmf205*$^{-/-}$ mice		
	(Chr 1) B6J/B6J	B6J/+	+/+
129S1/SvJ	11/11	0/20	0/11
A/J	9/9	0/22	0/8
AKR/J	6/6	0/11	0/5
C57BL6/NJ	6/6	0/14	0/8
CBA/J	7/7	0/10	0/7
DBA/2J	3/3	0/3	0/3
MA/MyJ	3/3	0/11	0/6
NODLt/2J	13/13	0/15	0/11

Table S1. Multiple strains carry the *Mod205* locus.
B6J-*nmf205*$^{+/-}$ mice were mated to wild-type (+/+) mice on various inbred strains and F1 mice were intercrossed. F2 mice were genotyped for the *nmf205* mutation and with polymorphic microsatellite or SNP markers in the *Mod205* region on Chromosome 1. Mice with recombination events in this region were removed from further analysis. F2 mice were accessed for ataxia and cerebellar degeneration at 7-8 weeks of age.

Strains	Experiments	Reads	P score	Footprint reads/codon
B6J.B6N$^{n\text{-}Tr20}$	replicate 1	28	7.94	0.65
B6J.B6N$^{n\text{-}Tr20}$	replicate 2	43	42.00	0.72
B6J	replicate 1	29	19.09	0.79
B6J	replicate 2	60	28.00	1.02
B6J.B6N$^{n\text{-}Tr20}$; *nmf205*$^{-/-}$	replicate 1	26	13.28	0.91
B6J.B6N$^{n\text{-}Tr20}$; *nmf205*$^{-/-}$	replicate 2	43	23.09	1.03
B6J-*nmf205*$^{-/-}$	replicate 1	61	20.41	1.16
B6J-*nmf205*$^{-/-}$	replicate 2	86	36.22	1.24

Table S3. Ribosome pausing on codon 256 of *Xbp1*.
The well-known ribosome pausing at codon 256 of *Xbp1* (references **16** and **17**) was observed in our study. The number of reads and pause (P) score at this codon and the footprint reads per codon on the *Xbp1* transcript, are shown for the 2 replicates of each strain. Strong pausing at this site is observed in all experiments, though the P score varies in magnitude. Assuming Poisson noise, the standard deviation of the number of reads across replicates is expected to be the square root of the number of reads, which is comparable in magnitude to the variations we observe across replicates.

Strains	Gene overlap between replicates	Excess gene overlap z-score	Codon overlap	Excess codon overlap z-score
B6J	12	17.9 (p<1e-200)	13	6.5 (p=4e-11)
B6J-*nmf205*$^{-/-}$	196	25.5 (p<1e-200)	254	13.9 (p=3e-44)

Table S4. Overlap of P≥10 AGA pauses across replicates.
Locations of AGA pauses were similar across replicates. In the two strains with increased AGA pausing (B6J and B6J-*nmf205*$^{-/-}$), we observed more overlap in genes with AGA pauses than expected by chance. In the B6J cerebellum we detected 12 genes with AGA pauses in common between replicates compared to 0.42 expected by chance. In the B6J-*nmf205*$^{-/-}$ cerebellum we detected 196 genes with AGA pauses in common vs 38.3 expected. We also observed significant overlap of the specific AGA codons with pauses in cerebellar replicates for strains with increased AGA pausing. In B6J cerebellar replicates we observed 13 overlapping AGA pause sites, which equates to an overrepresentation z-score=6.5 corresponding to p=4e-11. In B6J-*nmf205*$^{-/-}$ cerebellar replicates we observed 254 overlapping AGA pause sites, which equates to an overrepresentation z-score of 13.9 corresponding to p=3e-44.

References and Notes:

1. Genomic tRNA database. (http://gtrnadb.ucsc.edu).
2. J. M. Goodenbour, T. Pan, Diversity of tRNA genes in eukaryotes. *Nucleic Acids Res.* **34**, 6137-6146 (2006).
3. J. R. Buchan, I. Stansfield, Halting a cellular production line: responses to ribosomal pausing during translation. *Biol. Cell* **99**, 475-487 (2007).
4. S. D. Moore, R. T. Sauer, Ribosome rescue: tmRNA tagging activity and capacity in Escherichia coli. *Mol. Microbiol.* **58**, 456-466 (2005).
5. K. Rooijers, F. Loayza-Puch, L. G. Nijtmans, R. Agami, Ribosome profiling reveals features of normal and disease-associated mitochondrial translation. *Nat. Commun.* **4**, 2886 (2013).
6. D. Goldowitz *et al.*, Large-scale mutagenesis of the mouse to understand the genetic bases of nervous system structure and function. *Mol. Brain Res.* **132**, 105-115 (2004).
7. T. E. Dever, R. Green, The elongation, termination, and recycling phases of translation in eukaryotes. *Cold Spring Harb. Perspect. Biol.* **4**, a013706 (2012).
8. V. P. Pisareva, M. A. Skabkin, C. U. Hellen, T. V. Pestova, A. V. Pisarev, Dissociation by Pelota, Hbs1 and ABCE1 of mammalian vacant 80S ribosomes and stalled elongation complexes. *EMBO J.* **30**, 1804-1817 (2011).
9. C. J. Shoemaker, D. E. Eyler, R. Green, Dom34:Hbs1 promotes subunit dissociation and peptidyl-tRNA drop-off to initiate no-go decay. *Science* **330**, 369-372 (2010).
10. L. Levinger, D. Serjanov, Pathogenesis-related mutations in the T-loops of human mitochondrial tRNAs affect 3' end processing and tRNA structure. *RNA Biol.* **9**, 283-291 (2012).
11. L. Levinger, V. Vasisht, V. Greene, R. Bourne, A. Birk, S. Kolla, Sequence and structure requirements for Drosophila tRNA 5'- and 3'-end processing. *J. Biol. Chem.* **270**, 18903-18909 (1995).
12. H. Kudo, S. Senju, H. Mitsuya, Y. Nishimura, Mouse and human GTPBP2, newly identified members of the GP-1 family of GTPase. *Biochem. Biophys. Res. Commun.* **272**, 456-465 (2000).
13. M. Watanabe *et al.*, Cloning, expression analysis, and chromosomal mapping of GTPBP2, a novel member of the G protein family. *Gene* **256**, 51-58 (2000).
14. N. T. Ingolia, G. A. Brar, S. Rouskin, A. M. McGeachy, J. S. Weissman, The ribosome profiling strategy for monitoring translation in vivo by deep sequencing of ribosome-protected mRNA fragments. *Nat. Protoc.* **7**, 1534-1550 (2012).
15. N. T. Ingolia, S. Ghaemmaghami, J. R. Newman, J. S. Weissman, Genome-wide analysis in vivo of translation with nucleotide resolution using ribosome profiling. *Science* **324**, 218-223 (2009).
16. N. T. Ingolia, L. F. Lareau, J. S. Weissman, Ribosome profiling of mouse embryonic stem cells reveals the complexity and dynamics of mammalian proteomes. *Cell* **147**, 789-802 (2011).
17. K. Yanagitani, Y. Kimata, H. Kadokura, K. Kohno, Translational pausing ensures membrane targeting and cytoplasmic splicing of XBP1u mRNA. *Science* **331**, 586-589 (2011).

18. Materials and methods are available as supplementary material on Science Online.
19. N. R. Guydosh, R. Green, Dom34 rescues ribosomes in 3' untranslated regions. *Cell* **156**, 950-962 (2014).
20. T. Yagi, T. Tokunaga, Y. Furuta, S. Nada, M. Yoshida, T. Tsukada, Y. Saga, N. Takeda, Y. Ikawa, S. Aizawa, A novel ES cell line, TT2, with high germline-differentiating potency. *Anal. Biochem.* **214**, 70-76 (1993).
21. L. Zhao, C. Longo-Guess, B. S. Harris, J. W. Lee, S. L. Ackerman, Protein accumulation and neurodegeneration in the woozy mutant mouse is caused by disruption of SIL1, a cochaperone of BiP. *Nat. Genet.* **37**, 974-979 (2005).
22. M. V. Gerashchenko, A. V. Lobanov, V. N. Gladyshev, Genome-wide ribosome profiling reveals complex translational regulation in response to oxidative stress. *Proc. Natl. Acad. Sci. U.S.A.* **109**, 17394-17399 (2012).
23. R. Shalgi, J. A. Hurt, I. Krykbaeva, M. Taipale, S. Lindquist, C. B. Burge, Widespread regulation of translation by elongation pausing in heat shock. *Mol. Cell* **49**, 439-452 (2013).
24. W. Huang da, B. T. Sherman, R. A. Lempicki, Systematic and integrative analysis of large gene lists using DAVID bioinformatics resources. *Nat. Protoc.* **4**, 44-57 (2009).